

Triazaspirodimethoxybenzoyls as Selective Inhibitors of Mycobacterial Lipoamide Dehydrogenase^{†,‡}

Ruslana Bryk,[§] Nancy Arango,[⊥] Aditya Venugopal,^{§,Ⓜ} J. David Warren,^{||} Yun-Hee Park,[#] Mulchand S. Patel,[#] Christopher D. Lima,^{*,⊥} and Carl Nathan^{*,§,Ⓜ}

[§]Department of Microbiology and Immunology, and ^{||}Department of Biochemistry, Weill Cornell Medical College, New York, New York 10065, [⊥]Structural Biology Program, Sloan-Kettering Institute, New York, New York 10065, [Ⓜ]Program in Immunology and Microbial Pathogenesis, Weill Graduate School of Medical Sciences of Cornell University, New York, New York 10065, and [#]Department of Biochemistry, School of Medicine and Biomedical Sciences, University at Buffalo, The State University of New York, Buffalo, New York 14214

Received September 16, 2009; Revised Manuscript Received January 15, 2010

ABSTRACT: *Mycobacterium tuberculosis* (Mtb) remains the leading single cause of death from bacterial infection. Here we explored the possibility of species-selective inhibition of lipoamide dehydrogenase (Lpd), an enzyme central to Mtb's intermediary metabolism and antioxidant defense. High-throughput screening of combinatorial chemical libraries identified triazaspirodimethoxybenzoyls as high-nanomolar inhibitors of Mtb's Lpd that were noncompetitive versus NADH, NAD⁺, and lipoamide and >100-fold selective compared to human Lpd. Efficacy required the dimethoxy and dichlorophenyl groups. The structure of an Lpd–inhibitor complex was resolved to 2.42 Å by X-ray crystallography, revealing that the inhibitor occupied a pocket adjacent to the Lpd NADH/NAD⁺ binding site. The inhibitor did not overlap with the adenosine moiety of NADH/NAD⁺ but did overlap with positions predicted to bind the nicotinamide rings in NADH and NAD⁺ complexes. The dimethoxy ring occupied a deep pocket adjacent to the FAD flavin ring where it would block coordination of the NADH nicotinamide ring, while the dichlorophenyl group occupied a more exposed pocket predicted to coordinate the NAD⁺ nicotinamide. Several residues that are not conserved between the bacterial enzyme and its human homologue were predicted to contribute both to inhibitor binding and to species selectivity, as confirmed for three residues by analysis of the corresponding mutant Mtb Lpd proteins. Thus, nonconservation of residues lining the electron-transfer tunnel in Mtb Lpd can be exploited for development of species-selective Lpd inhibitors.

Most antibiotics with known mechanisms of action target bacterial synthesis of nucleic acids, protein, cell walls, or folate (1). The practice of focusing antibiotic development almost solely on these targets may have contributed to a steep decline in the rate of introduction of new anti-infectives, while emergence of drug resistance has continued unabated (2, 3). The need to identify inhibitors of new bacterial targets is particularly acute for tuberculosis (TB)¹. TB is second only to HIV as a leading cause of death from infectious disease and is the leading cause of death in people infected with HIV (4). TB cases resistant to all approved anti-infectives have been reported in 55 countries (5). TB chemotherapy is particularly challenging because therapy is more prolonged than for almost any other bacterial infection.

Prolonged therapy is required because some populations of Mtb are phenotypically tolerant to anti-infective agents that target pathways used by replicating Mtb to build biomass. Phenotypic tolerance is believed to arise when some of the bacteria persist in a nonreplicative state (6, 7).

New approaches have recently emerged in TB drug research. A diarylquinoline that inhibits ATP synthase was the first agent targeting bacterial energy production to enter clinical trials (8, 9). This agent is active against both replicating and nonreplicating Mtb, suggesting that energy production pathways can be effective targets in elimination of nonreplicators (10). The nitroimidazole PA-824 kills nonreplicating Mtb in part by generating reactive nitrogen species (11) that mimic an element of host immune chemistry (12). This underscores the possible utility of inhibiting Mtb's defenses against oxidative and nitrosative attack by the host (13, 14). We recently combined these approaches, that is, targeting both metabolic and detoxification pathways, in identifying inhibitors of Mtb's DltA (15), a component of Mtb's PDHC (16) and PNR/P (17, 18).

Here we have focused on Lpd as another enzyme that subserves both energy generation and defense against oxidative and nitrosative attack. Lpd (EC 1.8.1.4) belongs to a family of pyridine nucleotide:disulfide oxidoreductases and catalyzes flavin-dependent regeneration of the lipoamide cofactor involved in production of reducing equivalents in the form of a reduced cofactor (NADH). Lpd is a common component of eukaryotic and prokaryotic α -ketoacid dehydrogenase complexes, including

[†]This work was supported by National Institutes of Health Grants AI064768 and DK080748, the Milstein Program in Chemical Biology of Infectious Diseases, and the Milstein Chemistry Core Facility.

[‡]The atomic coordinates and structure factors have been deposited in the Protein Data Bank as entry 3II4.

*To whom correspondence should be addressed. C.N.: telephone, (212) 746-6505; fax, (212) 746-8587; e-mail, cnathan@med.cornell.edu. C.D.L.: telephone, (212) 639 8205; fax, (212) 717 3047; e-mail, limac@mskcc.org.

¹Abbreviations: Mtb, *Mycobacterium tuberculosis*; Lpd, lipoamide dehydrogenase; TB, tuberculosis; HIV, human immunodeficiency virus; PDHC, pyruvate dehydrogenase complex; PNR/P, peroxynitrite reductase/peroxidase; KGDHC, α -ketoglutarate dehydrogenase complex; BCKADHC, branched chain ketoacid dehydrogenase complex; GCS, glycine cleavage system; DltA, dihydrolipoamide acyltransferase; AhpD, alkyl hydroperoxide reductase protein D; DTNB, 5,5'-dithiobis-2-nitrobenzoic acid; OD, optical density.

PDHC, KGDHC, BCKADHC, and GCS. As the E3 component of PDHC, KGDHC, or BCKADHC complexes or the L-protein of the GCS, Lpd reoxidizes the lipoamide covalently attached to the ϵ -amino group of the active site lysine of the E2 components of α -ketoacid dehydrogenase complexes or the H-protein of the GCS and generates NADH. Each of these complexes functions at a critical commitment or regulatory step in intermediary metabolism.

Mtb's single functional Lpd is encoded by Rv0462 (19). The Mtb enzyme is a component of PDHC (16); however, Mtb lacks KGDHC (20), and until recently, no BCKADHC or GCS activities have been demonstrated in mycobacteria. Evidence that Mtb Lpd participates in BCKADHC will be presented elsewhere (A. Venugopal, R. Bryk, S. Ehrt, K. Rhee, and C. Nathan, manuscript in preparation). Unlike Lpd homologues from other species, Mtb Lpd is directly involved in protection against reactive nitrogen and reactive oxygen intermediates (18) as a component of an NADH-dependent PNR/P. The PNR/P complex also contains DlaT, the lipoamide-containing E2 component of PDHC; a thioredoxin-like protein specific to mycobacteria, termed AhpD; and the peroxiredoxin AhpC. As a component of PDHC, Lpd generates NADH via simultaneous oxidation of the lipoamide of DlaT. The PNR/P reaction proceeds in the opposite direction, and Lpd uses NADH to reduce DlaT's lipoamide and transfer reducing equivalents to AhpD's active site Cys and subsequently to regenerate reduced AhpC, which directly breaks down peroxynitrite and peroxides. Thus, mycobacterial Lpd uniquely links NADH-dependent metabolic and antioxidant pathways.

Mycobacteria lacking DlaT exhibited a delayed growth phenotype in vitro on carbohydrates as carbon source, were more susceptible to nitrosative stress than the wild type, and persisted in mouse lungs at $\sim 1.5 \log_{10}$ lower levels than the wild type, causing little histopathologic evidence of disease (21). Deficiency of Lpd imposes a much more severe phenotype on Mtb than deficiency of DlaT (A. Venugopal, R. Bryk, S. Ehrt, K. Rhee, and C. Nathan, manuscript in preparation). Thus, we reasoned that Mtb Lpd could be a better target than Mtb DlaT, provided that inhibitors of Mtb Lpd spare Lpd of the host. Although non-essential for in vitro growth of mycobacteria, both Δ dlaT and Δ lpd Mtb display an attenuated phenotype in vivo. Most strikingly, mice infected with Δ lpd Mtb exhibit no evidence of disease. Thus, while target validation is conventionally based on in vitro essentiality, we would argue that essentiality during infection of the host is the relevant criterion. The crystal structure of Mtb's Lpd (22) revealed active site differences between Mtb Lpd and human Lpd that might permit selective inhibition.

Here we present identification, characterization, and limited structure–activity relationship analysis of triazaspirodioxymethoxybenzoyls as potent, selective inhibitors of Mtb Lpd and report the cocrystal structure of Mtb Lpd with *N*-(2,4-dichlorophenethyl)-2-[8-(2,4-dimethoxybenzoyl)-4-oxo-1-phenyl-1,3,8-triazaspiro[4.5]decan-3-yl]acetamide (compound 5).

EXPERIMENTAL PROCEDURES

Materials. Bovine Lpd and porcine PDHC were from Sigma. 3-(4,5-Dimethylthiazol-2-yl)-5-(3-carboxymethoxyphenyl)-2-(4-sulfophenyl)-2H-tetrazolium assay reagents were from Promega. QuickChange site-directed mutagenesis kits were from Stratagene. NADH, DTNB, thiamine pyrophosphate, pyruvate, and all other reagents were from Sigma.

Proteins. Recombinant Mtb Lpd, DlaT, AhpD, and AceE were expressed without fusion tags in *Escherichia coli* and purified as described previously (16, 18, 19). Native bovine liver thioredoxin reductase was purified from calf liver as reported previously (23).

Overexpression and Purification of Human Lpd. A 5 mL overnight culture of *E. coli* M15 cells containing plasmid pDMI.1 and the pQE-9-E3 (Lpd) expression vector was used to inoculate a liter of LB medium containing ampicillin (100 μ g/mL) and kanamycin (25 μ g/mL). Cells were grown to an optical density of 0.7 and induced with isopropyl β -D-thiogalactopyranoside (200 μ g/mL) at 25 °C overnight. The cells were harvested by centrifugation at 6000g for 30 min at 4 °C, and the cell pellets were resuspended in 50 mM sodium phosphate (pH 8.0) containing 200 mM NaCl. Lysozyme was added to a final concentration of 1 mg/mL, and the suspension was incubated on ice for 30 min with occasional stirring. The cells were lysed in a French press (500 psi). Unbroken cells and debris were removed by centrifugation at 20000g for 30 min. The supernatant was applied to a Ni-nitrilotriacetic-agarose column. Lpd was eluted with a linear 30 to 150 mM imidazole gradient in 50 mM sodium phosphate (pH 8.0) containing 200 mM NaCl. Fractions containing human Lpd were dialyzed against 50 mM sodium phosphate buffer (pH 8.0) and stored at -80 °C (24). Human Lpd was $\sim 95\%$ pure as judged by densitometry of sodium dodecyl sulfate–polyacrylamide gel electrophoresis.

Preparation of D,L-Dihydrolipoamide. D,L-6,8-Thioctic acid (200 mg) was dissolved in 5 mL of a methanol/water mixture (4:1, v/v) at 50 °C. After solubilization, 1 mL of ice-cold sodium borohydride (200 mg/mL in water) was added and stirred for 1–2 h on ice (25). The solution was adjusted to pH 1.0–2.0 with 1 M HCl. The reduced compound was extracted with an equal volume of chloroform by shaking. The chloroform phase (lower layer) was transferred to a new container. This extraction procedure was repeated twice, and chloroform was evaporated using a Speed-Vac with heat. The white residue was resuspended with 10 mL of benzene, and then 4 mL of *n*-hexane was added immediately. The precipitate was collected when the solution was filtered through 3 MM paper and dried under vacuum. D,L-Dihydrolipoamide was stored at -20 °C with protection from light (26).

High-Throughput Screening. Screening was conducted in the Rockefeller University-Weill Medical College High Throughput Screening Resource Facility using 80000 compounds purchased from ChemDiv, Cerep, Spectrum, and Albany Molecular Research, Inc. As this collection grew, filters were applied for compounds with druglike properties and a lack of functionalities likely to promote nonspecific reactivity. Inhibition of DTNB reduction was assessed in Falcon Microtest 384-well plates with a capacity of 30 μ L per well. Lpd alone or together with DlaT and AhpD was dispensed in 10 μ L by a Matrix Wellmate plate filler. Compounds were added by a single dip (100 nL) with a Minitrak fluidics robot. Plates were incubated on a shaker for 30 min at room temperature. The reaction mixture [200 μ M NADH, 150 μ M DTNB in 100 mM potassium phosphate (pH 7.0), 2 mM ethylenediaminetetraacetic acid for the Lpd/DlaT/AhpD mixture, or including 150 μ M lipoamide for assays with Lpd alone] was added in 10 μ L volumes. The optical density at 405 nm due to 2-nitro-5-thiobenzoate (TNB) formation during DTNB reduction was recorded on an Envision Multifunction plate reader for “time zero” values. Plates were incubated on the shaker for 30 min at room temperature, and the

optical density at 405 nm was recorded again. Time zero values were subtracted from “time 30 min” values. The activity in control wells containing all components except test compounds was set to 100%. Wells with no protein but with the reaction mixture only were used as negative controls. The final concentrations of all components were as follows: Lpd (in complex or alone), 100 nM; DlaT, 175 nM; AhpD, 18 nM; NADH, 100 μ M; DTNB, 75 μ M; lipamide (if present), 75 μ M; potassium phosphate, 50 mM; ethylenediaminetetraacetic acid, 1 mM; test compounds, 12.5 μ M.

For hit confirmation, compounds were synthesized in house in the Milstein Chemistry Core Facility. Purity was >95% as assessed by nuclear magnetic resonance (Bruker DRX-500 spectrometer), high-performance liquid chromatography (Waters ACQUITY system), and electrospray ionization mass spectroscopy (Waters Micromass SQ spectrometer).

Enzymatic Assays. IC₅₀ values were determined with serial dilutions (100 to 0.1 μ M) of inhibitor by a fluorimetric assay with DTNB, lipamide, and NADH (19) or a PDHC assay (16) as described. Human Lpd was assayed by a DTNB assay with 10 μ M lipamide or a dihydrolipoamide-NAD⁺ spectrophotometric assay. Bovine thioredoxin reductase was assayed with 100 μ M NADPH and 75 μ M DTNB. NADH was detected by absorbance at 340 nm or fluorescence using a Molecular Devices SpectraMax M5 plate reader. Curves were fitted using IGOR Pro (WaveMetrics, Portland, OR) version 4.06A Carbon with the Hill equation, $Y = Y_{\max}/[1 + (IC_{50}/[I])^n]$, where n is the Hill coefficient. Kinetic parameters were determined by a NADH-lipoamide fluorimetric assay at variable substrate (from 0.2 to 5 mM lipamide; from 3.33 to 100 μ M NADH) and increasing inhibitor (0, 0.01, 0.1, 0.3, 0.6, 0.9, 1.2, and 2 μ M) concentrations in the presence of 20 μ M NAD⁺ to relieve inhibition by NADH and obtain hyperbolic plots (19) and by a dihydrolipoamide-NAD⁺ spectrophotometric assay at fixed dihydrolipoamide (1.5 mM), variable NAD⁺ (from 25 μ M to 2.5 mM), and increasing inhibitor (0, 1.2, 2, 4, and 8 μ M) concentrations. K_m and V_{\max} values were determined by fitting the data to hyperbolic function $V = V_{\max} \times X/(K_m + X)$. K_i values were determined from nonlinear regression analysis in Prism by fitting data to the equation for noncompetitive inhibition, $V = V_{\max}/(1 + I/K_i) \times X/(K_m + X)$.

Mammalian Cell Toxicity. Mouse bone marrow macrophages were isolated as reported previously (21), seeded at a density of 5×10^4 cells/well in a 96-well plate, and allowed to adhere for 24 h in Dulbecco's modified Eagle's medium with 4.5 g/L glucose, 0.584 g/L L-glutamine, 1 mM pyruvate, 10% fetal bovine serum, and 10% L-cell conditioned medium. The medium was then replaced with Dulbecco's modified Eagle's medium containing serial dilutions (from 100 μ M to 45 nM) of inhibitor. After 24 h, cell viability was assessed by reduction of 3-(4,5-dimethylthiazol-2-yl)-5-(3-carboxymethoxyphenyl)-2-(4-sulfophenyl)-2H-tetrazolium according to the manufacturer's instructions.

Site-Directed Mutagenesis. Site-directed mutagenesis was performed using the QuikChange kit. The following primers were used with the QuikStart MultiSite kit: 5'GCCGGAGCTGGT-GTAATTGGCATGGAGTTC3' (A181V), 5'CCGACCGCAA-GAGAATCGGTGTCGACG3' (A290R), and 5'CGGATG-TTGCCGTGACGTGACGTTCTGTCAGCC3' (R347S/A348V). The rest of the mutant Mtb Lpd proteins were made using the traditional QuikStart kit with the following primers: 5'ACCG-GCAGTAGCACCCTCTGGTTCCCGGCACC3' (forward)

and 5'AGGTGCCGGGAACCAGAGTGGTGCTACTGCCG-G3' (R147T) (reverse), 5'CGGGCGCTGCCCCGTTGAGGAC-GCCGATGTGTCC3' (forward) and 5'TTGGACACATCG-GCGTCCTCAACGGGCAGCGCCCCG3' (N209V) (reverse), 5'TTCCGCGGGCGCTGCCCCGTTATTGACGCCGATGTG-TCCAAGGAG3' (forward) and 5'CTTGGACACATCGGCG-TCAATAACGGGCAGCGCCCCGCGGAAGG3' (N209V/E210I) (reverse), 5'GCTATCGGCGATGTCAATGCTGGTCCAATG-CTGGCGCACGTGCGCGAGGC3' (forward) and 5'GCCTCG-GCGACGTGCGCCAGCATTTGGACCAGCATTGACATCGC-CGATAGC3' (G312A/L313G/L314P/Q315M) (reverse), 5'ATG-TCAATGGATTACCACAGCTGGCGCACGTCGCGCG3' (forward) and 5'CGGCGACGTGCGCCAGCTGTGGTAA-TCCATTGACAT3' (L314P) (reverse), 5'ACCATCGGATG-TTGCCGTGACGCGACGTTCTGTGTCAGCC3' (forward) and 5'GGCTGACAGAACGTCGCTGACGGCAACATCCATG-G3' (R347S) (reverse), and 5'AAGGTGTTGCAGGCCATC-GGACGAGCGCCCAACGTC3' (forward) and 5'GACGTT-GGGCGCTCGTCCGATGGCCTGCAACACCTT3' (F269R) (reverse). Mutant proteins were expressed and purified as described for wild-type Mtb Lpd (19).

Lysates were prepared as described previously (18), and protein was assessed by the Bradford method.

Cloning, Expression, and Protein Purification for Crystallization Analysis. Mtb *lpdC* (Rv0462)-(1–464) was amplified by polymerase chain reaction, cloned into a modified pET28b vector containing N-terminal hexahistidine-tagged *Saccharomyces cerevisiae* Smt3, and used to transform *E. coli* BL21(DE3) Codon Plus RLI (Novagen) as reported previously (22). A 6 L culture was fermented at 37 °C to an optical density of 0.8 at 600 nm, induced by addition of isopropyl β -D-thiogalactopyranoside to a final concentration of 1 mM, and then fermented at 30 °C for 4 h. Cells were harvested by centrifugation and suspended in 50 mM Tris-HCl (pH 8.0), 20% (w/v) sucrose, 350 mM NaCl, 20 mM imidazole, 0.1% *tert*-octylphenoxy poly(oxyethylene)ethanol, 1 mM phenylmethane-sulfonyl fluoride, 1 mM β -mercaptoethanol, and 10 μ g/mL DNase prior to sonication. Cell debris was removed by centrifugation. Protein was purified from the supernatant using Ni-NTA-agarose resin (Qiagen) and gel filtration (Superdex 200). The His₆-Smt3 tag was liberated from Mtb Lpd by incubation with Smt3 protease Ulp(403–621) (27), and the two proteins were separated by gel filtration (Superdex 200). Fractions containing Mtb Lpd were buffer exchanged into 20 mM Tris (pH 8.0), 87.5 mM NaCl, and 1 mM β -mercaptoethanol, concentrated to 10 mg/mL, aliquoted, flash-frozen in liquid nitrogen, and stored at –80 °C.

Crystallization and Structure Determination. Two hundred micromolar Mtb Lpd(1–464), 300 μ M compound 5, and 600 μ M NADH were mixed and incubated on ice for 10 min. Crystals were grown at 18 °C by hanging drop vapor diffusion against a well solution containing 100 mM Tris (pH 8.5), 10 mM NaCl, 11% polyethylene glycol 10000 (w/v), and 15% ethylene glycol (v/v). Crystals were further cryoprotected by being transferred to crystallization solutions containing the well solution with the addition of 25% ethylene glycol. Crystals were flash-cooled in liquid nitrogen. A single crystal was diffracted, and data were collected using a Rigaku RU200 X-ray generator equipped with confocal Osmic multilayer optics and a Raxis-IV imaging plate detector. A complete data set was obtained at 2.42 Å and reduced with DENZO, SCALEPACK, and CCP4 [Table 1 (28, 29)]. The same crystal was diffracted at NE-CAT beamline

Table 1: Data Collection and Refinement Statistics for Lpd-Compound **5** Cocrystal

Data Collection ^a	
space group	<i>P</i> 2 ₁ 2 ₁ 2 ₁
cell dimensions	
<i>a</i> , <i>b</i> , <i>c</i> (Å)	83.9, 98.4, 123.8
α , β , γ (deg)	90, 90, 90
resolution ^b (Å)	30–2.42 (2.51–2.42)
total no. of reflections	171989
no. of unique reflections	39154
Wilson <i>B</i>	37.3
<i>R</i> _{merge} ^b	8.0 (35.6)
<i>I</i> / σ <i>I</i> ^b	19.0 (3.7)
completeness ^b (%)	98.9 (98.0)
redundancy ^b	4.4 (3.6)
Refinement	
resolution ^b (Å)	30–2.42 (2.51–2.42)
no. of reflections <i>R</i> _{work} / <i>R</i> _{free}	37168/1942
<i>R</i> _{work} / <i>R</i> _{free} ^b	18.5 (25.2)/24.2 (31.1)
no. of atoms	
protein	6930
FAD	106
compound 5	86
water	751
average <i>B</i> factor	
protein (protomer A/B)	28.2/28.7
FAD (protomer A/B)	19.8/19.0
compound 5 (protomer A/B)	38.0/44.3
water	33.0
root-mean-square deviation	
bond lengths (Å)	0.006
bond angles (deg)	1.20

^aOne crystal. ^bValues for the highest-resolution shell given in parentheses.

24-IDC at 0.9795 Å, although no improvement in data quality was observed (not shown). The structure of Lpd bound to compound **5** was determined by molecular replacement using programs contained within CCP4 and our previously determined structure of Lpd (22). The crystal included one dimer in the asymmetric unit, and a model comprising Lpd amino acids 2–464 and 1–464 was refined after addition of 484 water molecules to *R* and *R*_{free} values of 0.21 and 0.27, respectively at 2.42 Å using CNS (30). A model for compound **5** was constructed using Chemdraw 3D and modeled using O (31) into 2*F*_o – *F*_c and *F*_o*F*_c electron density (Figure 1 of the Supporting Information). Stereochemical restraints for the model were modified on the basis of the electron density, and the final model was refined at 2.42 Å to *R* and *R*_{free} values of 0.19 and 0.24, respectively (Table 1). The model has excellent geometry with 89.3% of the residues in most favored, 10.7% of the residues in allowed, and no residues in generous or disallowed regions of the Ramachandran plot. The atomic coordinates and structure factors have been deposited in the Protein Data Bank (PDB) as entry 3II4.

RESULTS

Identification of Triazaspirodimeoxybenzoyls. We screened more than 80000 compounds using pure, recombinant, nontagged Mtb Lpd alone or in combination with pure, recombinant, nontagged DltA and AhpD (Figure 1). The screening was conducted via a DTNB reductase assay in which the generation of a yellow TNB product from DTNB occurs via sequential transfer of reducing equivalents from NADH via Lpd either to

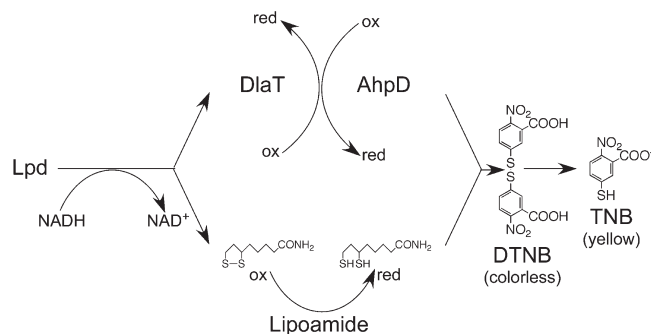


FIGURE 1: Schematic representation of the screening assay. Lpd reduces its substrate, lipoamide, at the expense of NADH, whether lipoamide is in solution or covalently attached to DltA (ox, oxidized; red, reduced). Lipoamide reduces DTNB to produce yellow TNB (Lpd-alone assay). DltA's reduced lipoamide reduces AhpD's active site Cys, which in turn reduces DTNB to produce yellow TNB (Lpd/DltA/AhpD assay). *Z'* factor values for both assays were 0.89–0.94.

lipoamide (when Lpd singularly was used in the assay) or to DltA to reduce its covalently attached lipoamide and then to the AhpD active site Cys. Either reduced lipoamide or reduced AhpD directly reduces DTNB to produce TNB. A set of 15000 compounds from ChemDiv was screened using the three-component protein mixture. Fourteen inhibitors were confirmed to inhibit Lpd when retested using Lpd alone. However, these were nonspecifically reactive in that they also inhibited thioredoxin reductase and were toxic to mammalian cells. It was then discovered that they underwent hydrolysis to maleimides. The remaining compounds from ChemDiv, Cerep, Spectrum, and Albany Molecular Research, Inc., were screened using Lpd alone. From the Spectrum library, 10 inhibitors that had nanomolar to low micromolar IC₅₀ values versus Mtb Lpd were identified, but they proved to be toxins such as phenylmercuric acetate, thimerosal, merbromin, hexachloropene, and cisplatin. Because screening of the first 20000 compounds with a criterion of 75% inhibition identified only redox-active and/or toxic compounds, we reduced the cutoff to 25% inhibition at 12.5 μM. With this criterion, the Albany Molecular Research, Inc., collection yielded 50 inhibitors (0.1% hit rate), of which 42 (84%) were confirmed upon retesting. Fifteen of these compounds inhibited Mtb Lpd with IC₅₀ values of < 50 μM. The most potent were triaza-spirodimeoxybenzoyls, whose activity was confirmed upon resupply, and compound **5**, described below, upon resynthesis in-house.

The most potent inhibitor, *N*-(2,4-dichlorophenethyl)-2-[8-(2,4-dimethoxybenzoyl)-4-oxo-1-phenyl-1,3,8-triazaspiro[4.5]-decan-3-yl]acetamide (compound **5**) (Figure 2A), had an IC₅₀ of 1 μM (*K*_i = 865 ± 41 nM) against Mtb Lpd and did not produce any measurable inhibition of human Lpd at concentrations up to 100 μM (Figure 2B,C). The structurally related inhibitor 2-[8-(2,4-dimethoxybenzoyl)-4-oxo-1-phenyl-1,3,8-triazaspiro[4.5]-decan-3-yl]-*N*-[3-(trifluoromethyl)benzyl]acetamide (compound **4**) had an IC₅₀ of 2 μM against Mtb Lpd and did not inhibit human Lpd at concentrations up to 100 μM (Table 2). Compounds **5** and **4** also inhibited Mtb Lpd in an NADH-lipoamide assay, a dihydrolipoamide-NAD⁺ assay, and a PDHC assay in complex with AceE and DltA, the E1 and E2 components of the PDHC. No inhibition of human Lpd at concentrations up to 100 μM was observed in the physiological direction of the reaction with dihydrolipoamide and NAD⁺ as substrates. Both compounds **5** and **4** efficiently inhibited Lpd activity in Mtb extracts with IC₅₀ values in the low micromolar range as measured

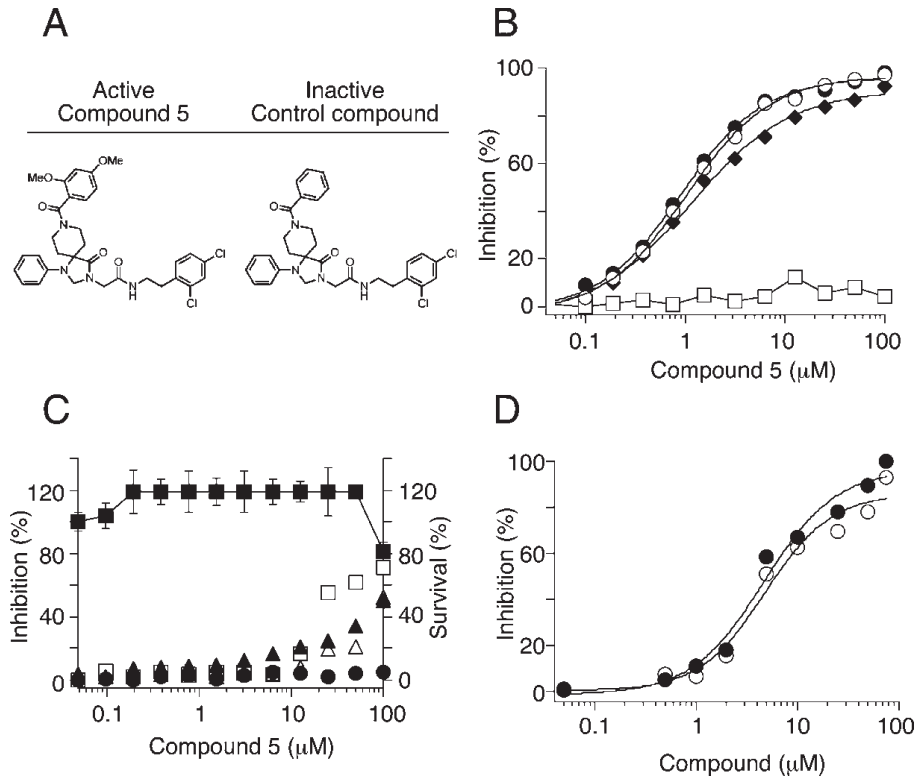
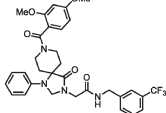
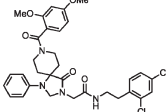
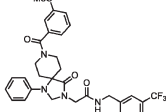


FIGURE 2: In vitro activities of triazaspirobenzoyls. (A) Chemical structures of active (compound **5**) and inactive triazaspirobenzoyl. (B) Compound **5** but not its congener lacking dimethoxy groups (\square) inhibits Mtb Lpd as measured by the DTNB assay without (\circ) or with 100 $\mu\text{g/mL}$ bovine serum albumin (\bullet) and by the NADH oxidase assay (\blacklozenge). (C) Compound **5** shows no inhibition vs human Lpd (\bullet) and minimally inhibits bovine Lpd (Δ), porcine PDHC (\blacktriangle), and bovine thioredoxin reductase (\square) and shows no toxicity against primary mouse bone marrow macrophages (\blacksquare). (D) Compounds **4** (\circ) and **5** (\bullet) inhibit PDHC activity in Mtb lysates.

Table 2: In Vitro Activities of Triazaspirobenzoyls^a

Structure	IC ₅₀ (μM)								
	Mtb Lpd	Mtb Lpd + BSA	Mtb Lpd NADH-lipoamide	Mtb PDHC	hLpd	bTR	bLpd	p PDHC	BMM EC ₅₀ (μM)
 compound 4	2.0	2.1	2.0	7.2	>100	>100	>100	100	>100
 compound 5	0.9	1.0	1.2	7.0	>100	20	100	100	>100
 compound 8	>100	>100	>100	not done	>100	25	>100	100	35

^aMtb Lpd activity was measured by DTNB, NADH-lipoamide, dihydrolipoamide-NAD⁺, and PDHC assays as described in Experimental Procedures. Bovine thioredoxin reductase (bTR), human (hLpd), and bovine (bLpd) Lpd activities were measured by the DTNB assay, and porcine PDHC (pPDHC) activity was measured by the PDHC assay and bone marrow macrophage (BMM) survival by the MTS assay. IC₅₀ values were determined by fitting data to the Hill equation in Igor Pro Carbon. EC₅₀ is the effective concentration at which viability is reduced to 50%.

by inhibition of PDHC activity (Figure 2D). Moreover, potency was unaffected in the presence of bovine serum albumin (100 $\mu\text{g/mL}$) (Figure 2B). Both compounds exhibited minimal activity with IC₅₀ values of ~ 100 μM against bovine thioredoxin reductase, a

redox enzyme belonging to the same family as Lpd, and affected mouse bone marrow macrophage survival only at the limit of solubility (100 μM , 80% survival) (Figure 2C). Triazaspirobenzoyls structurally similar to compounds **5** and **4** but lacking one or two

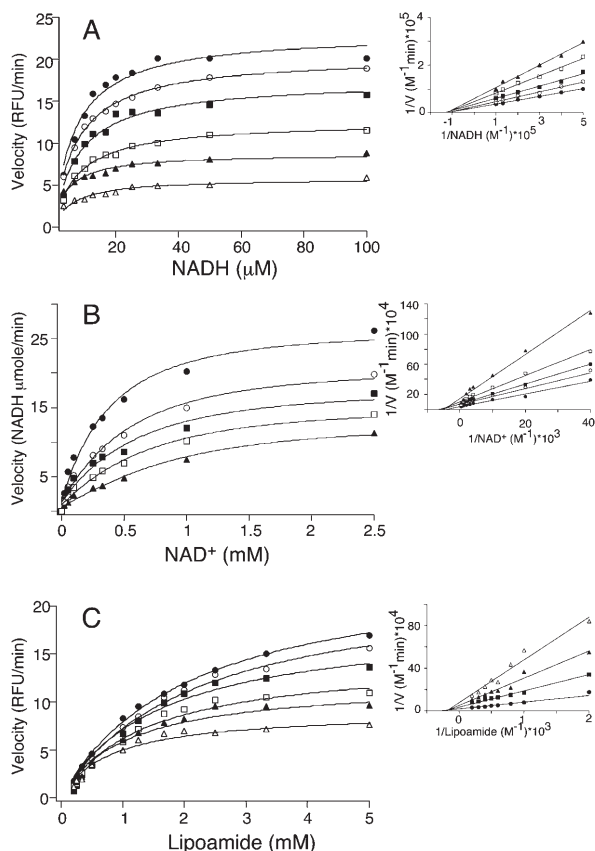


FIGURE 3: Compound **5** is noncompetitive vs NADH (A), NAD^+ (B), and lipoamide (C). The NADH-lipoamide fluorimetric assay used a variable concentration of NADH [(A) from 3.33 to 100 μM] or lipoamide [(C) from 0.5 to 5 mM], and the dihydrolipoamide- NAD^+ spectrophotometric assay used a variable concentration of NAD^+ [(B) from 25 μM to 2.5 mM] without inhibitor (●) or with an increasing level of compound **5** [(A) 10 nM (○), 300 nM (■), 600 nM (□), 900 nM (▲), and 2 μM (△), (B) 1.2 μM (○), 2 μM (■), 4 μM (□), and 8 μM (▲), and (C) 10 nM (○), 100 nM (■), 300 nM (□), 900 nM (▲), and 1.2 μM (△)]. Data were fitted in Prism to a nonlinear regression function for noncompetitive inhibition. Insets show double-reciprocal plots.

methoxy groups were inactive against Lpd and served as negative controls (Figure 2 and Table 2).

The mode of action of compound **5** was probed by varying the concentrations of the substrate (NADH, NAD^+ , or lipoamide) and inhibitor. The data suggested that compound **5** is non-competitive with respect to NADH, NAD^+ , and lipoamide (Figure 3).

We screened more than 300 triazaspiro compounds at 12.5 μM . The vast majority (>220) gave no inhibition of Mtb Lpd activity; 60 produced minimal (5–10%) inhibition, and 20 afforded inhibition in the range of 10–70%. Comparison of their structures revealed structure–activity relationships. Congeners lacking one or two methoxy groups were inactive (Table 3). Replacement of both methoxy groups with other groups such as trifluoromethyl led to a loss of activity. Triazaspirodimeethoxybenzoyls lacking the dichlorophenyl ethyl arm were inactive. Addition of a third methoxy to the latter compounds restored some activity but had no effect when added to compound **5**. Substitution of the dichlorophenyl ethyl with shorter substructures decreased activity; conversely, longer and bulkier groups produced better inhibition. Thus, both dimethoxybenzoyl and dichlorophenyl (trifluoromethylphenyl in compound **4**) groups appeared to be essential for inhibition of Mtb Lpd (Table 3).

Table 3: Structure–Activity Relationships of Selected Triazaspirobenzoyls^a

R_1	R_2	IC_{50} (μM)	Inhibition at 100 μM (%)
		0.9	100
		2.0	100
		>>100	12
		100	44
		100	46
		>100	29
		>100	40
		100	43
		>>100	10
		>>100	7
		>>100	0
		>>100	13
		>100	34
		0.9	100

^aMtb Lpd activity was measured by the DTNB assay. Data were fitted to the Hill equation in Igor Pro Carbon to determine IC_{50} values.

Intolerance to most substitutions suggested that the effective inhibitors engaged in specific, multipoint interactions with Mtb Lpd, indicative of binding in a protein pocket. Thus, we next sought to cocrystallize Mtb Lpd with compound **5**.

Structure of the Lpd–Compound 5 Complex. The protein component of the Mtb Lpd structure resembled that previously determined for Mtb Lpd in the absence of compound **5** with one Lpd dimer or two Lpd protomers in the crystallographic asymmetric unit (22). One inhibitor was observed in each Lpd protomer in a deep pocket adjacent to the FAD flavin ring and NADH/ NAD^+ binding pocket (Figure 4). Although 600 μM NADH was present in the crystallization and cryopreservation buffers, no NADH was observed in the structure, consistent with the binding of compound **5** (see below). The binding site occupied by compound **5** is proximal to the NAD^+ / NADH binding site and opposite the FAD ring with respect to the lipoamide binding site and active site cysteine residues (Cys41 and Cys46), which were observed in the oxidized, disulfide-bonded configuration.

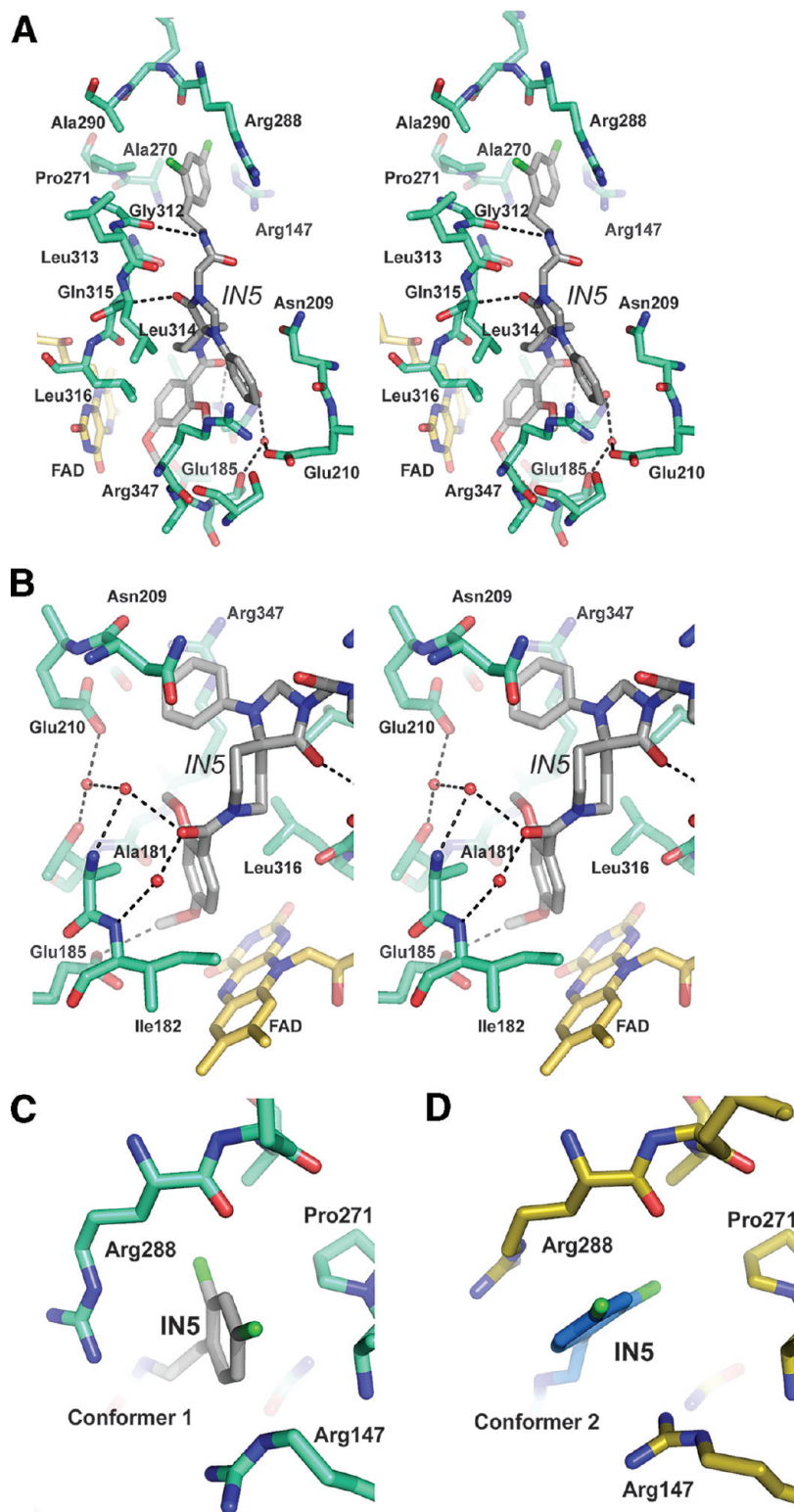


FIGURE 4: Schematic diagram of the complex between Mtb Lpd and compound **5**. (A) Stereoview of the structure of compound **5** (conformer 1) bound to Lpd (protomer A) with bonds and atoms shown in stick representation and color-coded with FAD carbon atoms colored yellow, protein carbon atoms blue, and compound **5** (IN5) atoms gray. Nitrogen atoms are colored dark blue and oxygen atoms red. Amino acid side chains are indicated by their three-letter amino acid code and numbered. Potential hydrogen bonding interactions are shown as dashed lines. Selected water molecules that mediate contacts to compound **5** are shown as red spheres. (B) Stereoview of an alternate close-up view of the structure of compound **5** (conformer 1) to illustrate interactions between the dimethoxybenzoyl ring and triazaspirophenyl core. Atoms are represented as in panel A. (C) Structure of the dichlorophenyl ring of compound **5** as coordinated in Lpd protomer A (conformer 1). Atoms represented in panel C are color-coded as described for panel A. (D) Structure of the dichlorophenyl ring of compound **5** as coordinated in Lpd protomer A (conformer 2). Atoms represented in panel D are color-coded with protein carbon atoms colored yellow and compound **5** carbon atoms dark blue. All depictions of the Lpd structure were generated using PyMol (45).

Compound **5** spans ~ 20 Å from the base of the dimethoxybenzoyl ring to the dichlorophenyl ring (Figure 4A) and buries

approximately 1300 Å² of total surface area in each of the two Lpd binding sites. The dimethoxybenzoyl ring is next to the FAD

flavin ring, and the oxygen from the proximal methoxy group is within 3.1 Å of the C4 atom of the flavin ring. The terminal carbon of the same methoxy group is also 3.1 Å from a carboxylate oxygen of Glu185. Additional interactions with the dimethoxy ring include van der Waals contacts between the dimethoxybenzoyl ring and side chain atoms of Leu316 and Ala181. The carbonyl oxygen atom adjacent to the dimethoxybenzoyl ring makes two water-mediated hydrogen bonds with the backbone amide atoms of amino acid residues Ala181 and Ile182, respectively (Figure 4B).

Interactions with the triazaspirophenyl core include van der Waals contacts between the phenyl ring and side chain atoms from amino acid residues Asn209, Glu210, and Arg347 (Figure 4B). Of these, the Arg347 aliphatic side chain and guanidinium group make the most extensive interactions with the phenyl ring of the triazaspirophenyl core. The carbonyl oxygen of the triazaspirophenyl core is also within hydrogen bonding distance (3.1 Å) of the backbone amide nitrogen of Gln315 (Figure 4A).

Several interactions were also observed between the protein and dichlorophenyl ring, including contacts to the linker between the triazaspirophenyl core and dichlorophenyl ring (Figure 4A). Electron density was notably weaker for the dichlorophenyl ring in both Lpd protomers (Figure 1 of the Supporting Information). In addition, the dichlorophenyl ring was observed in distinct conformations in each of the Lpd protomers (Figure 4C,D). In conformer 1 in Lpd protomer A, the carbonyl oxygen of amino acid residue Gly312 is within hydrogen bonding distance of the amide nitrogen in the linker between the triazaspirophenyl core and dichlorophenyl ring (Figure 4A,C). This contact was not observed in conformer 2 (Figure 4D). Interactions of the protein with the dichlorophenyl ring include van der Waals contacts with side chain atoms from Ala270, Pro271, Ala290, Arg147, and Arg288. The two conformations observed for the dichlorophenyl ring are accompanied by changes in the conformations of Arg147 and Arg288 in the two complexes (Figure 4C,D). The differences in dichlorophenyl ring conformations observed in the respective Lpd protomer might relate to differences in contacts to Lpd that are proximal to each binding site. The region of the Lpd structure around the binding site for compound **5** conformer 1 is fully exposed to solvent and not involved in lattice contacts, and while the region around the binding site of compound **5** conformer 2 is solvent-exposed, residues proximal to this binding site are near contacts to a symmetry mate that involves water-mediated lattice contacts to Asp287 and Lys289 and a direct lattice contact to a symmetry mate involving the Glu274 side chain. While these interactions do not involve residues that directly interact with compound **5**, additional contacts proximal to the ligand binding site might contribute to the conformation observed for compound **5** in this binding pocket.

The structure–activity relationships described above are consistent with the interactions observed in our crystal structure. One of the two methoxy groups of the dimethoxybenzoyl ring is within van der Waals distance of the flavin ring, consistent with the observation that congeners lacking one or two methoxy groups were inactive. The two conformations observed for the dichlorophenyl ring and accompanying changes in conformations for Arg147 and Arg288 are consistent with the ability to substitute the dichlorophenyl ring in compound **5** with the trifluoromethylphenyl ring in compound **4**. It is also consistent with the observation that substitution of the dichlorophenyl ethyl moiety with shorter substructures decreased activity; conversely, longer and bulkier groups produced better inhibition.

Compound 5 Partially Occludes Surfaces Important for Interaction with the Nicotinamide Ring of NAD. The surface pocket occupied by compound **5** partially overlaps with NAD⁺ and NADH cofactors as observed in complexes with human Lpd [Figure 5 (32)]. In the human Lpd structures, the adenosine monophosphate moiety of NAD occupies an exposed pocket comprised by side chains from Phe209, Glu208, Ile278, and Val243, which interact with the adenosine moiety while the monophosphate is coordinated by several backbone amide atoms (Figure 5A). The side chain composition and main chain composition of this binding site are strictly conserved with the Mtb Lpd enzyme [Phe202, Glu201, Ile267, and Val235 (22)]. In the human Lpd structures, the complexes differ, however, in the positions of the second phosphate and nicotinamide rings, depending on whether the enzyme is bound to NAD⁺ or NADH. In the NADH complex (Figure 5B,C), the second phosphate and nicotinamide ring penetrate into a deep pocket to stack the nicotinamide ring over the flavin ring in a configuration suitable for hydride transfer. In the NAD⁺ complex (Figure 5A,D), the second phosphate and nicotinamide ring occupy a solvent-exposed pocket. Superposition of the two human Lpd structures with our structure of the Mtb Lpd complex reveals that compound **5** would not occlude interactions with the surfaces involved in binding the NAD adenosine monophosphate moiety, but it would occlude surfaces predicted to be important for interactions with the nicotinamide ring in both NAD⁺ and NADH complexes. As discussed above, compound **5** exhibited noncompetitive inhibition with NADH and NAD⁺. Our structure and superimposition of NADH and NAD⁺ suggest that compound **5** binds within the NADH/NAD⁺ pocket. Thus, competitive behavior might be expected with respect to NADH/NAD⁺. However, since Lpd catalysis proceeds via a bisubstrate ping-pong bi-bi mechanism (33, 34), both competitive and noncompetitive inhibition patterns can be predicted (35) depending at which site and to which enzyme form the inhibitor will be binding. Lpd catalysis proceeds through two sequential steps of binding and release of products, while the enzyme oscillates between two forms, the reduced form with an NAD⁺ binding site and the oxidized form with an NADH binding site (Figure 2 of the Supporting Information). An inhibitor that binds exclusively to either the NAD⁺ or NADH binding site will be predicted to produce competitive kinetics with respect to the substrate of that site. However, an inhibitor that binds both NAD⁺ and NADH sites is expected to produce a noncompetitive pattern of inhibition versus both substrates, as predicted by Cleland (35). Thus, although a competitive pattern of inhibition against NAD⁺/NADH substrates may be expected from an inhibitor whose binding site overlaps partially with the NAD⁺/NADH site, its binding to both forms of the enzyme will result in the production of dead-end unproductive enzyme–inhibitor complexes for both forms. The resulting decrease in the amount of enzyme available to participate in catalysis will be manifested through a decrease in the apparent V_{\max} and the inability of an infinitely high substrate concentration to overcome the inhibition, thus leading to a noncompetitive inhibition pattern as observed.

Analysis of Mutant Lpd Proteins. Mutational analysis underscored the importance of contacts observed in the crystal structure and explained why compound **5** is a species-selective inhibitor of the Mtb Lpd enzyme. Our structural analysis confirmed that compound **5** makes multiple close contacts to main chain and side chain atoms within the Lpd active site pocket that were predicted to bind the nicotinamide ring of the

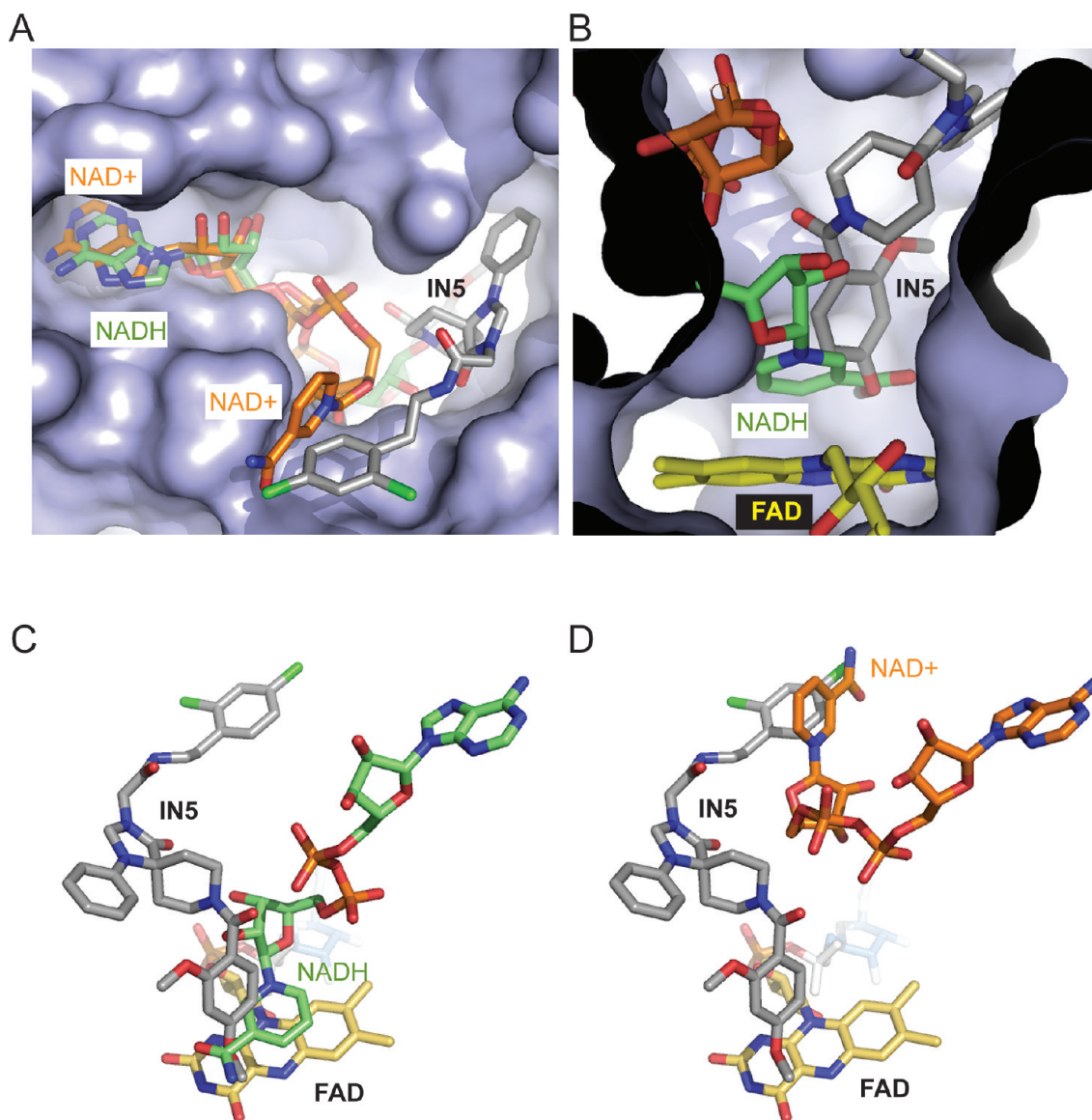


FIGURE 5: Compound **5** partially overlaps with NAD⁺/NADH cofactors. (A) Surface representation of Mtb Lpd in complex with compound **5** (conformer 1) with NAD⁺ and NADH cofactors superimposed on the structure as obtained by alignment of human Lpd structures in complex with NAD⁺ (PDB entry 1ZMC) and NADH (PDB entry 1ZMD) (32). The Lpd surface pocket that coordinates the adenosine monophosphate moiety of NAD⁺/NADH is highly conserved across evolution. NAD⁺ is labeled and shown with carbon atoms colored orange; NADH is labeled with carbon atoms colored green, and compound **5** (IN5) is labeled with carbon atoms colored gray. (B) Same as panel A, but a close-up view of the overlap between the nicotinamide ring of NADH and the dimethoxybenzoyl ring of compound **5** over the FAD cofactor. FAD carbon atoms are colored yellow, and carbon atoms for NADH and compound **5** are colored as in panel A. (C) View of NADH, compound **5**, and FAD in the absence of protein to illustrate the partial overlap between the NADH nicotinamide ring and the compound **5** dimethoxybenzoyl ring with carbon atoms color-coded as in panels A and B. (D) View of NAD⁺, compound **5**, and FAD in the absence of protein to illustrate the partial overlap between the NAD⁺ nicotinamide ring and the compound **5** dichlorophenyl ring with carbon atoms color-coded as in panels A and B.

NAD⁺/NADH cofactor. Alignment of the Mtb and human Lpd protein crystal structures (22, 32) showed that several amino acids in Mtb Lpd that contact the inhibitor are not conserved between the mycobacterial enzyme and its human homologue (Figure 5), although these residues are conserved among mammalian homologues (porcine and bovine Lpds). This prompted us to explore whether these amino acids may be responsible for the selectivity of compound **5** for the bacterial enzyme over its mammalian counterparts. We successfully produced eight recombinant mutant Mtb Lpd proteins (R147T, A181V, N209V, F269R, A290R, G312A/L313G/L314P/Q315M, L314P, and R347S), in which one or multiple residues of the mycobacterial Lpd were substituted with the corresponding residues of the human protein. The recombinant mutant Mtb Lpd proteins had V_{\max}

and K_m values comparable to those of the wild type in the absence of compound **5**. We were unable to purify four additional mutant proteins (N209V/E210I, E210I, R347S/A348V, and A348V) because when overexpressed in *E. coli*, they were retained in the insoluble fraction, suggesting that these substitutions resulted in protein misfolding and/or instability.

We tested the susceptibility of the purified mutant Mtb Lpd proteins to compound **5**. Substitution of the mycobacterial residues making contact with or in the proximity of the dichlorophenyl ring did not critically affect the activity of compound **5**, in that the IC_{50} of compound **5** was changed only slightly against mutant Lpd proteins R147T, F269R, and A290R, from 1 μ M (for the wild type) to 0.65–2 μ M (Table 4). In contrast, mutation of mycobacterial residue Ala181 whose side chain is within

3.4 Å of the dimethoxyphenyl ring (Figure 4B) to the corresponding Val of the human protein nearly abolished the activity of compound **5**, with only 10% inhibition at 100 μ M. Val is bulkier than Ala, suggesting that human Lpd protein might not be able to accommodate the inhibitor's dimethoxybenzoyl ring.

Mutation of the mycobacterial Leu314 whose side chain is within van der Waals distance of the triazaspirophenyl core (Figure 4A) also imparted resistance to the inhibitor (Table 4). However, mutation was tolerated at neighboring residues (G312, L313, and Q315) that made additional contacts with the compound's core, suggesting that substitution of Leu with Pro at this position introduced a more prominent change in the binding pocket. Similarly, substitution of Arg347 with Ser appeared to disrupt contact with the compound's phenyl ring projecting off the triazaspirophenyl core because this mutation conferred resistance to compound **5**. In contrast, Asn209, despite making multiple contacts with the same phenyl group, could be converted to Val without conferring resistance to compound **5**, suggesting that changing the polarity of the contact residue (substitution of Asn209 with Val) does not affect the binding of compound **5** but changing both the polarity and volume of the contact residue (substitution of Arg347 with Ser) produces a more drastic change within the binding pocket.

DISCUSSION

In the search for new antituberculosis chemotherapy, two approaches of interest are to identify compounds that can inhibit multiple targets or targets whose inhibition by a single compound can disrupt multiple pathways. There is more experience with the former approach. For example, isoniazid, the cornerstone of tuberculosis chemotherapy, has multiple targets (36). PA-824, a promising agent now in clinical trials, donates reactive nitrogen intermediates (11) that can react with multiple targets in Mtb (37, 38).

An example of the second approach—inhibition of one protein in Mtb, thereby disrupting more than one pathway—was perhaps first provided by the identification of species-selective thioxothiazolidines that inhibit Mtb DltA (15). This work provides another example, targeting Lpd, an enzyme that shares both of the known functions of DltA, in PDHC (16) and PNR/P (18), and serves at least one additional function as well, in BCKADHC (A. Venugopal, R. Bryk, S. Ehrhart, K. Rhee, and C. Nathan, manuscript in preparation).

Still more functions of bacterial Lpd are possible. While both bacterial and eukaryotic Lpds participate in major commitment steps of intermediary metabolism by regenerating the lipoamide cofactor covalently attached to the E2 subunit of α -ketoacid dehydrogenase complexes, Lpd in some bacteria has been implicated in galactose transport and α -galactoside metabolism (39) or found to be secreted and taken up by the host cell, where it may contribute to arrest of phagosome maturation (40). Archaea lack α -ketoacid dehydrogenase complexes yet still express Lpd (41), making it highly likely that certain Lpd homologues serve undiscovered functions. Among bacterial Lpds, mycobacterial Lpd appears to be unique in that it also fulfills an antioxidant function, helping to protect Mtb from reactive nitrogen and reactive oxygen intermediates (18).

Treatment of an infectious disease by targeting Lpd in the pathogen is not a new concept. Chagas' disease, caused by the protozoan *Trypanosoma cruzi*, was treated for many years with the nitrofurans nifurtimox (Lampit), which serves as a substrate that is cycled by the protozoal Lpd to generate reactive species

Table 4: Activity of Compound **5** against Mutant Mtb Lpd Proteins^a

Lpd protein	Contacts	IC ₅₀ (μ M)
Wild type		1
R147T		0.65
A181V		>>100
N209V		2
F269R		2
A290R		1.5
G312A L313G L314P Q315M		50
L314P		>50
R347S		>>100

^aMtb Lpd mutant proteins were generated and purified as described in Experimental Procedures. IC₅₀ values were determined with 100 nM protein in the DTNB assay. Red in the compound **5** structure denotes crystallographically evident contacts with Mtb Lpd; blue areas indicate contacts that were lost in a mutant Mtb Lpd.

harmful to the parasite (42). Nifurtimox is still used in the treatment of African sleeping sickness, caused by *Trypanosoma brucei*. To the best of our knowledge, however, no inhibitors of Lpd have previously been identified.

The likely impact of inhibiting Lpd in bacteria can be surmised from the phenotype of mutants in which the gene encoding Lpd has been disrupted. The phenotype of Lpd-deficient Mtb will be reported elsewhere (A. Venugopal, R. Bryk, S. Ehrt, K. Rhee, and C. Nathan, manuscript in preparation). *Streptococcus pneumoniae* deficient in Lpd was able to grow normally in vitro but was avirulent in sepsis and pneumonia models in mice (39). *Haemophilus influenzae* with a disrupted *lpd* gene was unable to establish infection in the rat (43). *Listeria monocytogenes* lacking an enzyme required for lipoylation of Lpd's interaction partner(s) in α -ketoacid dehydrogenase complexes was severely attenuated in mice (44).

Thus, bacterial Lpd is an attractive target for anti-infective agents, provided such agents spare Lpd of the host. Enzymes of intermediary metabolism are generally not considered as candidate targets for anti-infective therapy because of their high degree of conservation throughout evolution. Mycobacterial Lpd is 36% identical to the human homologue. Our studies demonstrate that it is possible to find species-selective inhibitors of mycobacterial Lpd. Several of the triazaspirodimethoxybenzoyls identified here are at least 100 times more selective for the bacterial enzyme than for the human enzyme.

Features critical for the potency and species selectivity of the triazaspirodimethoxybenzoyls include the dimethoxy substituents. Mutating amino acid residues of Mtb Lpd in contact with the dimethoxy groups to corresponding amino acids of the human enzyme conferred resistance to inhibition by triazaspirodimethoxybenzoyls. Trimethoxylated and dimethoxylated analogues of compound **5** were equally potent, suggesting that no additional contacts are made by a third methoxy group within the protein pocket. Moreover, conversion from the Mtb-encoded Leu314 to the human-encoded residue at the corresponding position apparently precluded productive contact with the triazaspirophenyl core of compound **5**, in that it led to a more than 100-fold decrease in inhibitory potency. Similarly, mutation of Arg347, which makes contact with the phenyl ring off the triazaspirocycle, to the corresponding Ser of the human protein decreased the potency of compound **5** by more than 100-fold.

Despite this evidence for tight binding of compound **5**, the cocrystal of Mtb Lpd with compound **5** revealed at least two positions for the dichlorophenyl ring along with compensatory changes in side chain positions of Arg147 and Arg288. While these data suggest some flexibility or plasticity in this region for both the inhibitor and protein, the dichlorophenyl functionality appeared to contribute to inhibition, because its removal resulted in a loss of inhibitory potency. Congeners with bulkier groups making closer contact with the protein in this region might improve the affinity or specificity of triazaspirodimethoxybenzoyls for Mtb Lpd.

To the best of our knowledge, this work is the first to identify inhibitors of Lpd in any species and the first to demonstrate that compounds can inhibit the Lpd of an infectious agent with potency orders of magnitude greater than that of the Lpd of its host. These results provide encouragement for seeking clinically useful Lpd inhibitors to target one protein serving diverse pathways in Mtb.

ACKNOWLEDGMENT

The Department of Microbiology and Immunology is supported by the William Randolph Hearst Foundation. We thank Ouathék Ouerfelli for discussion, Tarun Kapoor (Rockefeller University, New York, NY) for collaboration in the earliest phases of this work, and Charles Karan (Rockefeller University High Throughput Screening Resource Facility) for assembling compound collections. We thank the MSKCC X-ray core for use of their facility.

SUPPORTING INFORMATION AVAILABLE

Supplementary figures. This material is available free of charge via the Internet at <http://pubs.acs.org>.

REFERENCES

- Walsh, C. (2003) Where will new antibiotics come from? *Nat. Rev. Microbiol.* **1**, 65–70.
- Nathan, C. (2004) Antibiotics at the crossroads. *Nature* **431**, 899–902.
- Boucher, H. W., Talbot, G. H., Bradley, J. S., Edwards, J. E., Gilbert, D., Rice, L. B., Scheld, M., Spellberg, B., and Bartlett, J. (2009) Bad bugs, no drugs: No ESKAPE! An update from the Infectious Diseases Society of America. *Clin. Infect. Dis.* **48**, 1–12.
- World Health Organization (2008) <http://www.cdc.gov/hiv/resources/factsheets/hivtb.htm#1>.
- Donald, P. R., and van Helden, P. D. (2009) The global burden of tuberculosis: Combating drug resistance in difficult times. *N. Engl. J. Med.* **360**, 2393–2395.
- Levin, B. R., and Rozen, D. E. (2006) Non-inherited antibiotic resistance. *Nat. Rev. Microbiol.* **4**, 556–562.
- Warner, D. F., and Mizrahi, V. (2006) Tuberculosis chemotherapy: The influence of bacillary stress and damage response pathways on drug efficacy. *Clin. Microbiol. Rev.* **19**, 558–570.
- Andries, K., Verhasselt, P., Guillemont, J., Gohlmann, H. W., Neefs, J. M., Winkler, H., Van Gestel, J., Timmerman, P., Zhu, M., Lee, E., Williams, P., de Chaffoy, D., Huitric, E., Hoffner, S., Cambau, E., Truffot-Pernot, C., Lounis, N., and Jarlier, V. (2005) A diarylquinoline drug active on the ATP synthase of *Mycobacterium tuberculosis*. *Science* **307**, 223–227.
- Diacon, A. H., Pym, A., Grobusch, M., Patientia, R., Rustumjee, R., Page-Shipp, L., Pistorius, C., Krause, R., Bogoshi, M., Churchyard, G., Venter, A., Allen, J., Palomino, J. C., De Marez, T., van Heeswijk, R. P., Lounis, N., Meyvisch, P., Verbeeck, J., Parys, W., de Beule, K., Andries, K., and Mc Neeley, D. F. (2009) The diarylquinoline TMC207 for multidrug-resistant tuberculosis. *N. Engl. J. Med.* **360**, 2397–2405.
- Koul, A., Vranckx, L., Dendouga, N., Balemans, W., Van den Wyngaert, I., Vergauwen, K., Gohlmann, H. W., Willebrords, R., Poncelet, A., Guillemont, J., Bald, D., and Andries, K. (2008) Diarylquinolines are bactericidal for dormant mycobacteria as a result of disturbed ATP homeostasis. *J. Biol. Chem.* **283**, 25273–25280.
- Singh, R., Manjunatha, U., Boshoff, H. I., Ha, Y. H., Niyomrattanakit, P., Ledwidge, R., Dowd, C. S., Lee, I. Y., Kim, P., Zhang, L., Kang, S., Keller, T. H., Jiricek, J., and Barry, C. E., III (2008) PA-824 kills nonreplicating *Mycobacterium tuberculosis* by intracellular NO release. *Science* **322**, 1392–1395.
- MacMicking, J. D., North, R. J., LaCourse, R., Mudgett, J. S., Shah, S. K., and Nathan, C. F. (1997) Identification of nitric oxide synthase as a protective locus against tuberculosis. *Proc. Natl. Acad. Sci. U.S.A.* **94**, 5243–5248.
- Nathan, C., Gold, B., Lin, G., Stegman, M., de Carvalho, L. P., Vandal, O., Venugopal, A., and Bryk, R. (2008) A philosophy of anti-infectives as a guide in the search for new drugs for tuberculosis. *Tuberculosis* **88** (Suppl. 1), S25–S33.
- Lin, G. L. D., Sorio de Carvalho, L. P., Deng, H., Tao, H., Vogt, G., Wu, K., Schneider, J., Chidawanyika, T., Warren, J. D., Li, H., and Nathan, C. (2009) Inhibitors selective for mycobacterial versus human proteasomes. *Nature* **461**, 621–626.
- Bryk, R., Gold, B., Venugopal, A., Singh, J., Samy, R., Pupek, K., Cao, H., Popescu, C., Gurney, M., Hotha, S., Cherian, J., Rhee, K., Ly, L., Converse, P. J., Ehrt, S., Vandal, O., Jiang, X., Schneider, J., Lin, G., and Nathan, C. (2008) Selective killing of nonreplicating mycobacteria. *Cell Host Microbe* **3**, 137–145.

16. Tian, J., Bryk, R., Shi, S., Erdjument-Bromage, H., Tempst, P., and Nathan, C. (2005) *Mycobacterium tuberculosis* appears to lack α -ketoglutarate dehydrogenase and encodes pyruvate dehydrogenase in widely separated genes. *Mol. Microbiol.* 57, 859–868.
17. Bryk, R., Griffin, P., and Nathan, C. (2000) Peroxynitrite reductase activity of bacterial peroxiredoxins. *Nature* 407, 211–215.
18. Bryk, R., Lima, C. D., Erdjument-Bromage, H., Tempst, P., and Nathan, C. (2002) Metabolic enzymes of mycobacteria linked to antioxidant defense by a thioredoxin-like protein. *Science* 295, 1073–1077.
19. Argyrou, A., and Blanchard, J. S. (2001) *Mycobacterium tuberculosis* lipoamide dehydrogenase is encoded by Rv0462 and not by the lpdA or lpdB genes. *Biochemistry* 40, 11353–11363.
20. Tian, J., Bryk, R., Itoh, M., Suematsu, M., and Nathan, C. (2005) Variant tricarboxylic acid cycle in *Mycobacterium tuberculosis*: Identification of α -ketoglutarate decarboxylase. *Proc. Natl. Acad. Sci. U.S.A.* 102, 10670–10675.
21. Shi, S., and Ehrt, S. (2006) Dihydrolipoamide acyltransferase is critical for *Mycobacterium tuberculosis* pathogenesis. *Infect. Immun.* 74, 56–63.
22. Rajashankar, K. R., Bryk, R., Kniewel, R., Buglino, J. A., Nathan, C. F., and Lima, C. D. (2005) Crystal structure and functional analysis of lipoamide dehydrogenase from *Mycobacterium tuberculosis*. *J. Biol. Chem.* 280, 33977–33983.
23. Holmgren, A. (1977) Bovine thioredoxin system. Purification of thioredoxin reductase from calf liver and thymus and studies of its function in disulfide reduction. *J. Biol. Chem.* 252, 4600–4606.
24. Liu, T. C., Korotchikina, L. G., Hyatt, S. L., Vettakkorumakankav, N. N., and Patel, M. S. (1995) Spectroscopic studies of the characterization of recombinant human dihydrolipoamide dehydrogenase and its site-directed mutants. *J. Biol. Chem.* 270, 15545–15550.
25. Reed, L. J., Koike, M., Levitch, M. E., and Leach, F. R. (1958) Studies on the nature and reactions of protein-bound lipoic acid. *J. Biol. Chem.* 232, 143–158.
26. Patel, M. S., and Hong, Y. S. (1998) Lipoic acid as an antioxidant: Methods in molecular biology, Humana Press Inc., Totowa, NJ.
27. Mossessova, E., and Lima, C. D. (2000) Ulp1-SUMO crystal structure and genetic analysis reveal conserved interactions and a regulatory element essential for cell growth in yeast. *Mol. Cell* 5, 865–876.
28. Otwinowski, Z., and Minor, W. (1997) *Methods Enzymol.* 276, 307–326.
29. Collaborative Computational Project, Number 4 (1994) The CCP4 suite: Programs for protein crystallography. *Acta Crystallogr. D* 50, 760–763.
30. Brunger, A. T., Adams, P. D., Clore, G. M., DeLano, W. L., Gros, P., Grosse-Kunstleve, R. W., Jiang, J. S., Kuszewski, J., Nilges, M., Pannu, N. S., Read, R. J., Rice, L. M., Simonson, T., and Warren, G. L. (1998) Crystallography & NMR system: A new software suite for macromolecular structure determination. *Acta Crystallogr. D* 54, 905–921.
31. Jones, T. A., Zou, J. Y., Cowan, S. W., and Kjeldgaard, M. (1991) Improved methods for building protein models in electron density maps and the location of errors in these models. *Acta Crystallogr. A* 47 (Part 2), 110–119.
32. Brautigam, C. A., Chuang, J. L., Tomchick, D. R., Machius, M., and Chuang, D. T. (2005) Crystal structure of human dihydrolipoamide dehydrogenase: NAD⁺/NADH binding and the structural basis of disease-causing mutations. *J. Mol. Biol.* 350, 543–552.
33. Massey, V., Gibson, Q. H., and Veege, C. (1960) Intermediates in the catalytic action of lipoyl dehydrogenase (diaphorase). *Biochem. J.* 77, 341–351.
34. Reed, J. K. (1973) Studies on the kinetic mechanism of lipoamide dehydrogenase from rat liver mitochondria. *J. Biol. Chem.* 248, 4834–4839.
35. Cleland, W. W. (1963) The kinetics of enzyme-catalyzed reactions with two or more substrates or products. II. Inhibition: Nomenclature and theory. *Biochim. Biophys. Acta* 67, 173–187.
36. Argyrou, A., Jin, L., Siconolfi-Baez, L., Angeletti, R. H., and Blanchard, J. S. (2006) Proteome-wide profiling of isoniazid targets in *Mycobacterium tuberculosis*. *Biochemistry* 45, 13947–13953.
37. Nathan, C. (2008) Microbiology. An antibiotic mimics immunity. *Science* 322, 1337–1338.
38. Reed, K. Y., Erdjument-Bromage, H., Tempst, P., and Nathan, C. F. (2005) S-Nitroso proteome of *Mycobacterium tuberculosis*: Enzymes of intermediary metabolism and antioxidant defense. *Proc. Natl. Acad. Sci. U.S.A.* 102, 467–472.
39. Smith, A. W., Roche, H., Trombe, M. C., Briles, D. E., and Hakansson, A. (2002) Characterization of the dihydrolipoamide dehydrogenase from *Streptococcus pneumoniae* and its role in pneumococcal infection. *Mol. Microbiol.* 44, 431–448.
40. Deghmane, A. E., Soualhine, H., Bach, H., Sendide, K., Itoh, S., Tam, A., Noubir, S., Talal, A., Lo, R., Toyoshima, S., Av-Gay, Y., and Hmama, Z. (2007) Lipoamide dehydrogenase mediates retention of coronin-1 on BCG vacuoles, leading to arrest in phagosome maturation. *J. Cell Sci.* 120, 2796–2806.
41. Danson, M. J. (1988) Dihydrolipoamide dehydrogenase: A 'new' function for an old enzyme? *Biochem. Soc. Trans.* 16, 87–89.
42. Viode, C., Bettache, N., Cenas, N., Krauth-Siegel, R. L., Chauviere, G., Bakalara, N., and Perie, J. (1999) Enzymatic reduction studies of nitroheterocycles. *Biochem. Pharmacol.* 57, 549–557.
43. Herbert, M., Kraiss, A., Hilpert, A. K., Schlor, S., and Reidl, J. (2003) Aerobic growth deficient *Haemophilus influenzae* mutants are non-virulent: Implications on metabolism. *Int. J. Med. Microbiol.* 293, 145–152.
44. O'Riordan, M., Moors, M. A., and Portnoy, D. A. (2003) *Listeria* intracellular growth and virulence require host-derived lipoic acid. *Science* 302, 462–464.
45. Delano, W. L. (2002) The PyMOL molecular graphics system, DeLano Scientific, San Carlos, CA.